Available online at www.sciencedirect.com
SCIENCE DIRECT®
ELSEVIER
Nuclear Instruments and Methods in Physics Research A 520 (2004) 27–31
NUCLEAR INSTRUMENTS & METHODS IN PHYSICS RESEARCH Section A
www.elsevier.com/locate/nima

Metallic magnetic calorimeters (MMC): detectors for high-resolution X-ray spectroscopy

A. Fleischmann[a,*], M. Link[a], T. Daniyarov[a], H. Rotzinger[a], C. Enss[b], G.M. Seidel[b]

[a] *Kirchhoff-Institut für Physik, Universität Heidelberg, INF 227, Heidelberg D-69120, Germany*
[b] *Department of Physics, Brown University, Box 1843, Providence, RI 02912, USA*

Abstract

X-ray detectors based on the concept of magnetic calorimetry are well suited for high-resolution spectroscopy. Metallic magnetic calorimeters (MMC) make use of a metallic paramagnetic temperature sensor, which is in tight thermal contact with a metallic X-ray absorber. The paramagnetic sensor is placed in a small magnetic field. Its magnetization is used to monitor the temperature, which in turn is related to the internal energy of the calorimeter. High-energy resolution can be obtained by using a low-noise, high-bandwidth DC SQUID to measure the small change in magnetization upon the absorption of an X-ray. With recent prototype detectors an energy resolution of $\Delta E_{\mathrm{FWHM}} = 3.4$ eV for X-ray energies up to 6.5 keV has been achieved. We discuss general design considerations, the thermodynamic properties of such calorimeters, the energy resolution, and the various sources of noise, which are observed in MMCs.

PACS: 07.85.Fv; 85.25.Oj; 85.25.Dq

Keywords: Low-temperature particle detectors; SQUID's; Magnetic susceptibility

1. Introduction

The detection of a particle with a metallic magnetic calorimeter (MMC) is based on the measurement of the change of magnetization of a metallic paramagnetic sample sitting in a small magnetic field. This change of magnetization is proportional to the temperature change caused by the absorption of the particle. A magnetic calorimeter consists of an absorber suited for stopping the particle to be detected and a paramagnetic sensor that is thermally coupled to the absorber. To obtain high sensitivity a DC SQUID is used to measure the magnetization.

Metallic sensors are used to achieve fast thermalization at operating temperatures well below 100 mK [1]. In recent years the physics of one system, gold doped with erbium, has been studied extensively [2,3]. Based on a detailed knowledge of Au:Er it is possible to optimize the performance of an MMC employing this material as a sensor. Given the temperature of operation and the heat capacity of the absorber, the values of the adjustable parameters, magnetic field, dimen-

*Corresponding author.
E-mail address: andreas.fleischmann@kip.uni-heidelberg.de (A. Fleischmann).

0168-9002/$ - see front matter © 2003 Elsevier B.V. All rights reserved.
doi:10.1016/j.nima.2003.11.212

sions of the sample and erbium concentration can be calculated to maximize the signal.

2. Experimental technique

2.1. Detector design

The magnetic calorimeter in these studies consists of two Au:Er sensors with a separate X-ray absorber attached to each of them. The sensors were laser-cut discs, 50 μm in diameter and 25 μm thick, made of Au containing 300 ppm of isotopically enriched ^{166}Er. To stop 6 keV X-rays from a ^{55}Fe source 150 μm × 150 μm × 5 μm gold foils were used as absorbers. The quantum efficiency for 6 keV X-rays of this thickness of Au is higher than 98%. These absorber foils were attached to the Au:Er sensors using a wedge bonder. The completed sensor/absorber sandwiches were positioned manually into the two loops of a SQUID gradiometer [6,7] and were held in place with a thin layer of vacuum grease.

2.2. Two-stage SQUID readout

A two-stage DC SQUID system was employed in this experiment, consisting of a primary detector SQUID and a secondary amplifier SQUID. Because of the absence of an on-chip field coil capable of producing a field localized to the sensors, the entire SQUID chip with Josephson junctions was located in a magnetic field of about 3 mT. The magnetic field reduces the critical current of the SQUID by almost a factor of eight. In turn, the peak-to-peak voltage is reduced to 7.5 μV and the slope of the characteristic curve becomes 21 $\mu V/\Phi_0$. If the detector SQUID were read out with room temperature electronics having a pre-amplifier noise of 0.3 $nV/\sqrt{Hz}$, the apparent flux noise level would be 15 $\mu\Phi_0/\sqrt{Hz}$. At this white noise level the performance of our detectors would be significantly degraded. To reduce the white noise level in our experiments we have used a second SQUID as a voltage amplifier. A schematics of the circuit diagram of the two-stage SQUID system is shown in Fig. 1.

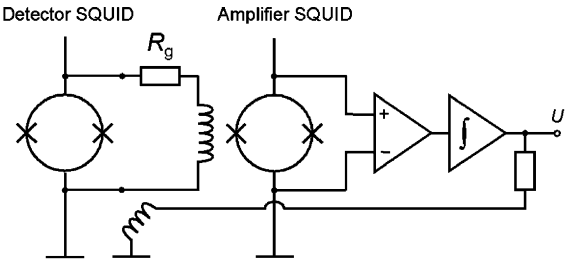

Fig. 1. Schematic circuit diagram of the two-stage SQUID system.

The double-stage SQUID system has a common feedback loop. The gain is determined by the resistor R_g. To achieve stable operation the flux gain between the SQUIDs was chosen to be about 3. For gains larger than 4 the U–Φ-characteristic becomes very complex and, in particular, exhibits multiple working points with different slopes. At a gain of 3, the maximum slope of the characteristic curve becomes 600 $\mu V/\Phi_0$ and the white-noise level of the two-stage SQUID is 0.5 $\mu\Phi_0/\sqrt{Hz}$.

Due to the relatively weak feedback coupling of the detector SQUID the slew rate of the two-stage system is only about 0.1 $\Phi_0/\mu s$. This slew rate is not sufficient to follow the fast rise of the signal and therefore the rise time of the pulses in our experiment is determined by the SQUID electronics. As a side effect this limits the usable signal size to about 0.6 Φ_0.

2.3. Data acquisition and analysis

The analog output signal of the SQUID electronics was digitized by a 12-bit AD converter and subsequently processed. For each event, traces of 16 k samples were acquired. Besides the actual X-ray events, an equivalent number of randomly triggered baseline traces were recorded.

The pulse height of individual events was determined by applying an optimal filter. The filter function was obtained in the usual way by calculating the signal responsivity and the spectral noise density and constructing a weighting function. The optimal filter function was Fourier transformed back to the time domain and the height of an individual pulse was determined by

the convolution of the single pulse with this filter function.

3. Results and discussion

3.1. Resolving power

The detector described in Section 2.1 was cooled to a temperature of about 35 mK and its performance tested using a ^{55}Fe source. A typical spectrum of the source is shown in Fig. 2. It contains the K_α and K_β lines of ^{55}Mn. Due to the high quantum efficiency of the gold absorber the spectrum is very clean indicating that very few events are not associated with the expected lines. The trigger level was set at about 100 eV in this experiment.

The inset of Fig. 2 shows an unfiltered single pulse. In the actual experiment a 10 Hz high pass and a 10 kHz low pass was used. The rise time of the signal is about 5 μs and, as stated before, is determined by the slew rate of the SQUID system.

The thermalization time is about 60 ms due to the weak coupling to the thermal bath via vacuum grease.

To determine the instrumental resolution of our detector we have used the K_α line and fitted it with the line-shape determined using a crystal spectrometer.

The experimental spectrum is best described with an instrumental resolution of 3.4 eV. Fig. 3 shows a blow-up of the K_α line data together with the theoretical spectrum accounting for the natural and instrumental linewidth.

Using the same instrumental resolution one also can describe satisfactorily the K_β line. Fig. 4 shows the K_β line together with the theoretical spectrum.

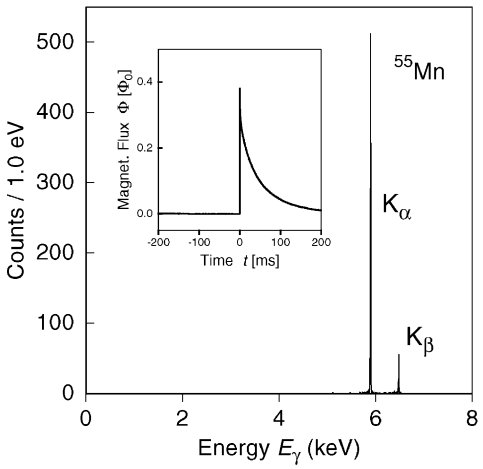

Fig. 2. X-ray spectrum of ^{55}Mn.

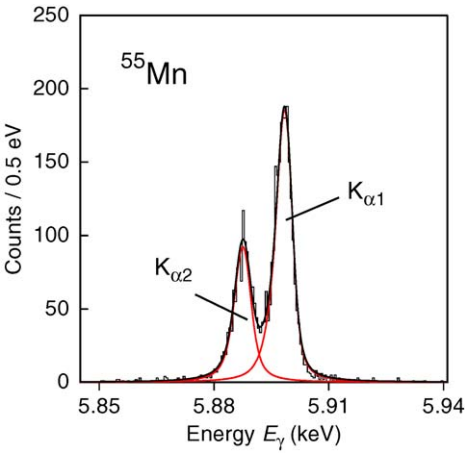

Fig. 3. K_α line of ^{55}Mn. The solid line represents a fit of the data taking into account the natural linewidth as determined with a crystal spectrometer [4].

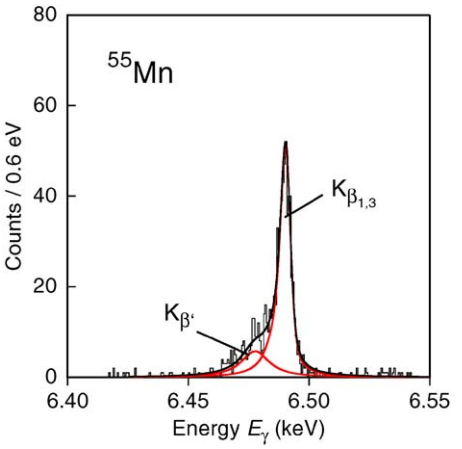

Fig. 4. K_β line of ^{55}Mn. The solid line represents a fit of the data taking into account the natural linewidth as determined with a crystal spectrometer [4].

Recently, it has been shown that the shape of the K_β line of ^{55}Mn depends strongly on the chemical composition in which the manganese is present [5]. The shape of the K_β line measured in our experiment is consistent with the fact that our source is made of metallic ^{55}Fe.

3.2. Noise

To evaluate the random noise contribution to our instrumental resolution, we have analyzed the baseline traces. The result is shown in Fig. 5.

The fact that the width of this histogram is 3.26 eV and thus is very close to the instrumental resolution of 3.4 eV indicates that random noise dominates the resolution of our detector.

The expected noise from intrinsic thermodynamic fluctuations is small. Since the heat capacity of the absorbers plus sensors in the two loops is approximately 3×10^{-12} J/K at 35 mK the noise contribution of thermodynamic fluctuations should be only 0.7 eV. Here we have taken the ratio of rise time and thermalization time to be 3×10^{-5}. The difference between the measured baseline noise and the thermodynamic fluctuations consists of two components, white noise and $1/f$ noise. A noise spectrum for our detector under operational conditions is shown in Fig. 6. The white-noise level is about 1.4 $\mu\Phi_0/\sqrt{\text{Hz}}$. It has two contributions, the flux noise of the detector SQUID of 1.1 $\mu\Phi_0/\sqrt{\text{Hz}}$ and the magnetic Johnson noise of the sensor of 0.9 $\mu\Phi_0/\sqrt{\text{Hz}}$.

The noise spectrum at low frequencies can only in part be explained by the contribution of thermodynamic fluctuations. In addition, $1/f$ noise appears in our experiment. Surprisingly, this noise component is temperature independent in the experimental range from 30 mK to 4 K. Fig. 7 shows the noise spectrum of our set-up without the contribution of thermodynamic fluctuations at

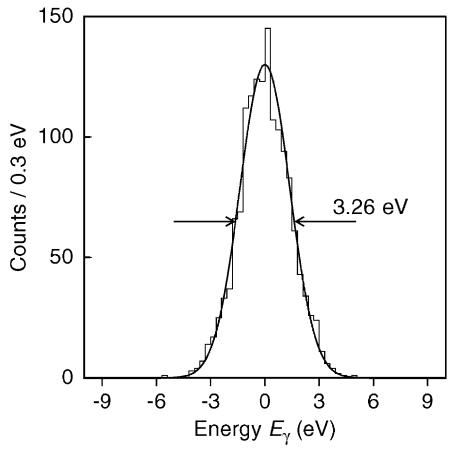

Fig. 5. Histogram resulting from the analysis of baseline traces.

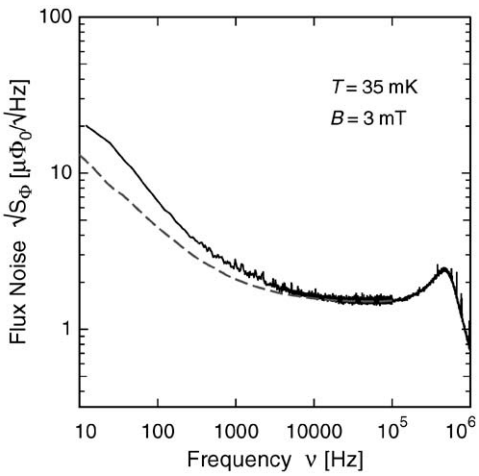

Fig. 6. Noise spectrum of our detector taken under operational conditions.

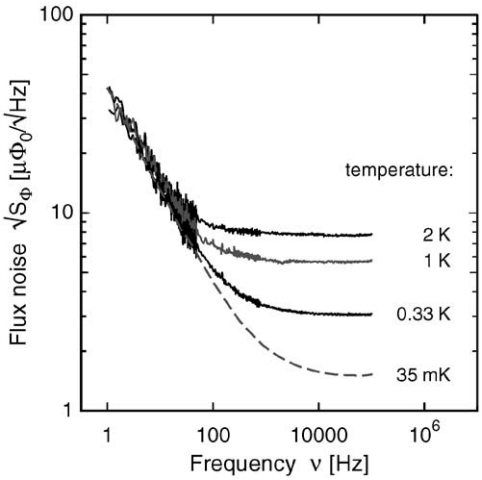

Fig. 7. Noise spectra of our detector at different temperatures in zero magnetic field.

different temperatures. Here the $1/f$ component is clearly visible. The white noise level varies proportionally to $\sqrt{T}$ as expected. Although we do not know the origin of the $1/f$ noise, it is associated with the presence of the spins in the sensor. A pure gold sample, when substituted for the sensor, does not show the effect. At this point we can only speculate about the physical nature of the $1/f$ noise. One possibility might be hierarchical relaxations within the interacting spin system. Whether this is, in fact, the case remains to be determined by further experiments.

Acknowledgements

We thank S. Hunklinger, R. Stolz and V. Zakosarenko for stimulating discussions. This work was supported by the DFG (Grant En299/3), BMBF (Grant F&E 13N8226) and NASA (Grant NAG5-10383).

References

[1] S.R. Bandler, C. Enss, R.E. Lanou, H.J. Maris, T. More, F.S. Porter, G.M. Seidel, J. Low Temp. Phys. 93 (1993) 709.
[2] A. Fleischmann, J. Schönefeld, J. Sollner, C. Enss, J.S. Adams, Y.H. Kim, S.R. Bandler, G.M. Seidel, J. Low Temp. Phys. 118 (2000) 7.
[3] C. Enss, A. Fleischmann, K. Horst, J. Schönefeld, J. Sollner, J.S. Adams, Y.H. Huang, Y.H. Kim, G.M. Seidel, J. Low Temp. Phys. 121 (2000) 137.
[4] G. Hölzer, M. Fritsch, M. Deutsch, J. Hartwig, E. Förster, Phys. Rev. A 56 (1997) 4554.
[5] K. Sakurai, H. Eba, Nucl. Instr. and Meth. B 199 (2003) 391.
[6] M.B. Ketchen, D.D. Awschalom, W.J. Gallagher, A.W. Kleinsasser, R.L. Sandstrom, J.B. Rosen, B. Bumble, IEEE Trans. Magn. 25 (1989) 1212.
[7] G.K. Stawiasz, B.M. Ketchen, R.L. Narasimhan, IEEE Trans. Appl. Supercond. 5 (1989) 3230.